Int. J. Electrochem. Sci., 14 **(2019)** 387 – 401, doi: 10.20964/2019.01.37

International Journal of
ELECTROCHEMICAL
SCIENCE
www.electrochemsci.org

S-containing Molybdenum Oxide Films as pH Neutral Hydrogen Evolution Electrocatalyst prepared by Electrodeposition

Rasa Mardosaitė[*], *Eugenijus Valatka*

Department of Physical and Inorganic Chemistry, Kaunas University of Technology, Radvilenu str. 19, LT-50254 Kaunas, Lithuania.
[*]E-mail: rasa.mardosaite@ktu.lt

Received: 9 September 2018 / *Accepted:* 18 October 2018 / *Published:* 30 November 2018

Molybdenum sulfides, molybdenum oxides, and S-containing molybdenum oxides have been shown to be promising electrocatalysts for hydrogen evolution. In this context, amorphous Mo–O–S films on a fluorine-doped tin oxide (FTO) substrate were prepared by cyclic voltammetry using two different electrodeposition baths containing different Mo and S precursors. Although ammonium tetrathiomolybdate (ATTM) was successfully used as a source for Mo and S, this precursor was identified as having some limitations. Therefore, an alternative electrodeposition bath containing thiourea and ammonium molybdate was presented in this work. Amorphous thiourea-molybdate-based films were annealed under an inert atmosphere, and the thermal effect was subsequently evaluated by X-ray diffraction (XRD), Fourier transform infrared spectroscopy (FT-IR), scanning electron microscopy (SEM), energy dispersive X-ray spectroscopy (EDS), UV-Vis, and Raman analysis. Finally, harsh galvanostatic electrolysis conditions were applied to perform a preliminary evaluation of the catalytic behaviour of the Mo–O–S films in a phosphate buffer solution (pH 7). The Mo–O–S films prepared from the thiourea-molybdate bath showed promising stability and activity results, with a Tafel slope of 85 $mV \cdot dec^{-1}$ in the range of overpotentials lower than 100 mV even after prolonged HER operation. These findings open an alternative approach to the possible mechanism of Mo–O–S formation.

Keywords: molybdenum oxide; molybdenum sulfide; thiourea; electrodeposition; hydrogen evolution reaction

1. INTRODUCTION

Zero-carbon and hydrogen rich fuels have historically been considered an ideal advanced and innovative type of energy [1]:

C (coal) → -CH_2- (oil) → CH_4 (natural gas) → H_2 (hydrogen)

However, the energy used today is still based on fossil fuels, which were stored naturally over millions of years. Therefore, humans are accustomed to paying only the mining costs of fossil fuels. In order to shift the world to a synthetic fuel like hydrogen, the economy must first be convinced to pay for H_2 production. In this regard, water electrolysis would be one of the most economically and environmentally friendly, renewable, and clean methods to produce hydrogen. Tremendous efforts have been made to find alternative earth-abundant inorganic hydrogen evolution catalysts to replace Pt, which is scarce, expensive, and unattractive for large scale applications [2, 3].

Molybdenum sulfides prepared either as nanoparticles or as films are very attractive noble-metal-free electrocatalysts for the hydrogen evolution reaction (HER) from water. Crystalline molybdenum disulfide (*c*-MoS_2), amorphous molybdenum sulfide (*a*-MoS_x), and molybdenum sulfide molecular clusters have gained attention for their scalable preparation methods, attractive catalytic activities, and robustness, especially in harsh H_2-evolving conditions [4]. Various Mo-S film structures can be obtained, as molybdenum has oxidation states ranging from –2 to +6 and coordination numbers from 0 to 8 [5]. Amorphous molybdenum sulfide is known to exhibit significantly higher HER activity compared to its crystalline counterpart, likely due to a higher amount of unsaturated Mo and S sites. Although amorphous molybdenum sulfides lack long-range order, they contain short-range atomic arrangements which are electrocatalytically active [6].

Generally, the electrodeposition of Mo-S films involves the use of ammonium tetrathiomolybdate (ATTM, $(NH_4)_2MoS_4$). The electrolytic reduction of tetrathiomolybdate (MoS_4^{2-}) to give MoS_2 may proceed in a similar manner to the well-known reduction of molybdate (MoO_4^{2-}) to MoO_2 [7]. A number of publications have reported the electrodeposition of Mo-S films from ATTM by cyclic voltammetry and potentiostatic electrolysis techniques.

Cyclic voltammetry in an aqueous solution of ATTM has been successful for various conductive substrates, such as fluorine-doped tin oxide (FTO), indium tin oxide (ITO), and glassy carbon (GC) electrodes. A mixture of amorphous MoS_3, MoS_2, and other sulfur species were found to be deposited [6, 8, 9]. Secondly, constant anodic and cathodic potential electrolysis were employed to deposit films on an FTO substrate from aqueous ammonium tetrathiomolybdate solutions. The two potentiostatic methods yielded films with different proportions of amorphous MoS_3 and MoS_2 phases. The amorphous MoS_3 film was not stable in 1 M KOH and quickly dissolved in the electrolyte, while the MoS_{2+x} composition was stable in alkaline solutions [9, 10].

To the best of our knowledge, reports of the electrodeposition of Mo-S without using ATTM are limited. After a review of related studies, we noted that room temperature ionic liquids and high-temperature molten salts, particularly, were employed for nonaqueous electrodeposition of Mo-S [11, 12], while MoO_4^{2-} was generally found to be employed in the majority of aqueous electrolytes.

The fact that the electrodeposition potential of Mo is more negative than the discharge potential of hydrogen creates difficulties in the cathodic electrodeposition of Mo-S films from aqueous solutions. Furthermore, molybdenum compounds are known to be easily oxidized, and oxides form inevitably on their surface [5]. In terms of redox chemistry, MoO_4^{2-} is believed to be the dominant Mo species in aqueous solution. It should be noted that the redox behaviour, charge, coordination, and ionic radii of MoO_4^{2-} are similar to those of SO_4^{2-} [13].

In the context of the chalcogenide family, MoO_4^{2-} is typically used as a Mo source for the preparation of films of molybdenum selenides [14, 15]. However, only a few successful attempts of the electrodeposition of MoS_2 in a similar manner to that of $MoSe_2$, i.e., using MoO_4^{2-} as a simple, stable, and widely available Mo precursor, have been reported. In these reports, an aqueous solution of Na_2MoO_4 and Na_2S with hydrochloric acid was used, which probably resulted in the formation of tetrathiomolybdate via chemical reaction in the deposition bath. Potentiostatic deposition was performed, and amorphous films containing Mo, S, and appreciable amounts of oxygen were obtained as a result of the aqueous room temperature electrodeposition. Annealing of these films in an inert atmosphere resulted in the formation of highly-textured films of MoS_2 with van der Waals planes parallel to the substrate. As oxygen was an inevitable component of the deposits, the electrodeposited material was later identified as molybdenum oxosulfides [7, 16].

Na_2MoO_4 and Na_2S were again used as the Mo and S precursors with sulfuric acid as the pH regulator. Various substrates were found to be suitable for the deposition. The electrochemical reduction of thiomolybdate, which was chemically derived from the precursors, was detected at a potential of about –0.3 V vs. Ag/AgCl, and the deposited material was identified as MoS_x [17].

A two-step electrochemical/chemical method was employed to synthesize molybdenum disulfide nanostructures. First, amorphous MoO_x was potentiostatically electrodeposited by an electrochemical step-edge decoration technique from a basic aqueous solution of Na_2MoO_4. Subsequently, the MoO_x precursors were chemically converted to MoS_2 by heating in a tube furnace at 500–1000 °C under flowing H_2S [18].

Clearly, a great deal of further investigation into the use of alternative Mo and S precursors (i.e. other than ATTM) in the electrochemical synthesis of amorphous molybdenum sulfides remains to be done. Previous experimental work has revealed that ATTM has some limitations as a Mo and S precursor. Before electrolysis, its stability is problematic due to the oxidation of Mo and S species in aqueous solutions under an air atmosphere. Furthermore, we noticed that during electrolysis the surfaces of electrochemical cell were covered with a thin layer of unidentified and very difficult to remove residues. Thus, the development of alternative electrolysis bath is highly desired in order to make the synthesis more economical and environmental friendly.

The aim of this work was to form S-containing molybdenum oxide films on FTO glass substrates using the electrochemical deposition method, and to study the structure and electrocatalytic activity of the resulting films in aqueous neutral phosphate solutions. In this work, we suggest for the first time an alternative electrodeposition bath containing thiourea (TU) and ammonium molybdate as the S and Mo sources, respectively. Based on the successful use of thiourea in the aqueous electrodeposition of cobalt–sulfide films, TU was chosen as the sulfur donor for the molybdenum-containing bath. We predicted that thiourea might be able to act as a S source for Mo-based films based on the report of Arvia et al. [19]. They proposed that the electro-oxidation/reduction and electro-adsorption/desorption of thiourea molecules could lead to the extensive sulfidation of metal surfaces. Eventually, we adopted the terminology “S-containing oxide films” and employed it to represent the samples prepared in this work.

2. EXPERIMENTAL

2.1. Preparation of S-containing molybdenum oxide films

The electrodeposition of S-containing molybdenum oxide (denoted as Mo–O–S throughout the paper) films was performed using two different Mo and S precursor baths: (A) ammonium tetrathiomolybdate (ATTM; $(NH_4)_2MoS_4$), and (B) a solution of thiourea (TU; $SC(NH_2)_2$) and ammonium molybdate ($(NH_4)_6Mo_7O_{24}$).

Thiourea ($SC(NH_2)_2$, ≥99%, Sigma Aldrich), ammonium molybdate tetrahydrate ($(NH_4)_6Mo_7O_{24}\cdot 4H_2O$, ≥99%, Reachem) and ammonium tetrathiomolybdate (ATTM; $(NH_4)_2MoS_4$, 99.94%, Sigma Aldrich) were used as supplied without further purification.

Cyclic voltammetry was employed for the electrodeposition of the films on the FTO substrate. Prior to deposition, the fluorine-doped tin oxide (FTO) glass substrates (TEC15, 3.5 × 1 cm, 13 Ω sq^{-1}) were cleaned successively using a soap solution, deionized water, and acetone in an ultrasonic bath. The thus-prepared FTO plates were used as working electrodes in a thermostated three electrode cell with Ag, AgCl| $KCl_{(sat)}$ as a reference electrode and platinum wire (geometric area about 15 cm^2) as a counter electrode. The working and counter compartments of the cell were separated by the frit. All three electrodes were placed in a 100-mL deposition bath filled with solutions of the Mo–O–S precursors. The ATTM-derived films were deposited by 20 sweep-cycles at a scan rate of 50 mV/s from an electrolysis bath containing 0.005 M ATTM and 0.1 M $NaClO_4$. Three sweep-cycles were applied for the Mo–O–S samples deposited from an electrolysis bath containing 0.5 M thiourea and 0.005 M ammonium molybdate at a scan rate 5 mV/s. For both types of Mo–O–S films, the potential was cycled from –1.2 V to 0.2 V vs. Ag/AgCl. During all the experimental runs, intense brownish films were obtained as a result of electrodeposition. The as-synthesized samples were thoroughly washed with distilled water and dried at room temperature.

The thiourea-molybdate based Mo–O–S films were additionally annealed at 623 K for 3 h under a flow of nitrogen. The freshly prepared and thermally treated samples were then analysed using structural analysis techniques.

2.2 Analytical techniques

The electrochemical properties of the potentiodynamically deposited Mo–O–S samples were evaluated using a computer–controlled VSP (BioLogic Science Instruments, France) potentiostat/galvanostat connected to a three-electrode cell. EC-Lab V10.39 software was used for the collection and treatment of experimental data. The FTO/Mo–O–S sample was used as the working electrode, a platinum wire as the counter electrode, and Ag, AgCl| $KCl_{(sat)}$ as the reference electrode. All the electrochemical tests were performed in a 1 M potassium phosphate buffer solution (pH 7) under an air atmosphere.

A polycrystalline platinum plate (geometrical surface area 2 cm^2) was also polarized in the phosphate buffer solution and used as a benchmark for comparison with the prepared Mo–O–S samples.

X-ray diffraction (XRD) patterns were recorded on a D8 Advance diffractometer (Bruker AXS, Karlsruhe, Germany) with CuKα radiation. The Mo–O–S film specimens were scanned over the range $2\theta = 5–70°$ at a scanning speed of 6° min^{-1} using a coupled two theta/theta scan type.

Fourier transform infrared (FT-IR) spectra of the samples were recorded on a Perkin Elmer FT–IR Spectrum X System. KBr was used to pellet the samples, and the scans were conducted over a 400–4000 cm^{-1} scanning range.

Examination of the surface morphology and elemental composition of the FTO/Mo–O–S samples was performed using a Quanta FEG 200 (FEI) high resolution scanning electron microscope (SEM) equipped with a detector (Bruker AXS) for high resolution energy dispersive X-ray spectroscopy (EDS).

Raman scattering measurements were performed using an *inVia* Raman microscope (Renishaw). The excitation beam from a diode laser with a wavelength of 532 nm was focused on the sample using a 50× objective (NA = 0.75, Leica). The laser power on the sample surface was varied from 0.35 mW to 3.5 mW. The integration time was 5–10 s, and the signal was accumulated 1–5 times and then averaged. The Raman Stokes signal was dispersed using a diffraction grating (2400 grooves/mm), and data was recorded using a Peltier-cooled charge-coupled device (CCD) detector (1024 × 256 pixels). This system yields a spectral resolution of about 1 cm^{-1}. Silicon was used to calibrate both the wavenumber and spectral intensity of the Raman setup.

UV-Vis diffuse reflectance (UV-Vis DR) spectra of the samples were recorded using a Lambda 35 UV–Vis spectrometer (Perkin Elmer Instruments Co. Ltd., USA) equipped with a 50-mm machined Spectralon® integrating sphere. A $BaSO_4$ disc was employed as a reference. The scan ranged from 200 to 800 nm.

The thickness of the as-deposited films was measured using an Ambios XP-200 profilometer.

3. RESULTS AND DISCUSSION

3.1 Electrodeposition of Mo–O–S films

Optimized cyclic voltammetry (CV) was used to prepare thin Mo–O–S films on the FTO substrates from the two different electrolysis baths, and the results are shown in Fig. 1. For the ATTM-derived films (Fig. 1-a), the electrolysis bath and potential cycling window were adapted based on the Mo–O–S deposition regime [9]. Therefore, the potential was cycled from 0.2 V to –1.2 V and one reduction and one oxidation peak were observed at –0.8 and –0.2 V, respectively. A homogeneous brownish film layer was deposited on the glass substrate after the 20 continuous sweep cycles. The obtained experimental results were in good agreement with the proposed mechanism of film formation (eqs. (1)–(3)) [6, 8]. The anodic peak at –0.2 V can be assigned to the oxidation of aqueous MoS_4^{2-} followed by MoS_3 deposition, as described in equation (1). When the potential was cycled in reverse from 0.2 V in the negative direction, reductive corrosion was found to consume about 70% of the previous deposits via the reaction in equation (2). Finally, the cathodic peak at –0.8 V may indicate the further reduction of MoS_4^{2-} to form amorphous MoS_2, SH^-, and OH^- (eq. (3)). According to this mechanism, potential cycling of a MoS_4^{2-} solution would always produce a molybdenum sulfide film

that is a mixture of amorphous MoS_3, MoS_2, other sulfur species, and the inevitably formed oxo compounds.

$$MoS_4^{-2} \rightarrow MoS_3 + \frac{1}{8}S_8 + 2e^- \quad (1)$$

$$MoS_3 + \frac{1}{8}S_8 + 2e^- \rightarrow MoS_4^{-2} \quad (2)$$

$$MoS_4^{-2} + 2H_2O + 2e^- \rightarrow MoS_2 + 2HS^- + 2OH^- \quad (3)$$

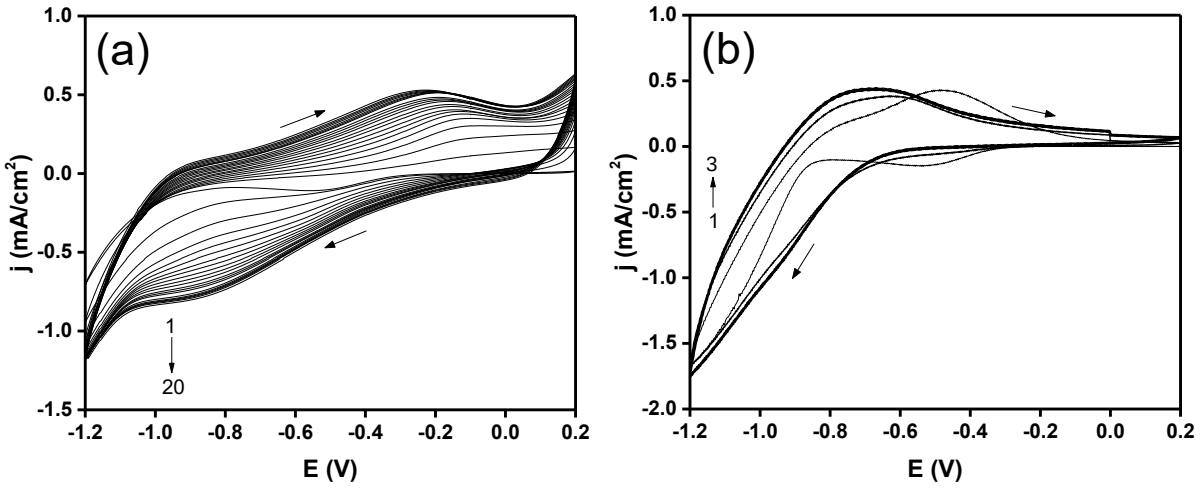

Figure 1. Characteristic cyclic voltammograms of Mo–O–S deposition on FTO. (a) 20 sweep-cycles in an electrolysis bath containing 0.005 M ATTM and 0.1 M $NaClO_4$ and (b) 3 sweep-cycles in an electrolysis bath containing 0.5 M thiourea and 0.005 M ammonium molybdate

For the thiourea and molybdate electrolysis bath, the FTO electrode was cycled continuously from 0.2 V to –1.2 V until a thin layer of brownish film was observed to deposit on the working electrode after three sweep cycles. Profilometry measurements revealed that the thickness of the as-deposited films after three sweep cycles using the thiourea–molybdate bath was 245 nm; this value was more than 100 nm greater than that of the ATTM-derived films deposited after 20 cycles. It should also be noted that the synthesis from an ATTM-based electrolysis bath was previously reported to have an upper film thickness limit of less than 200 nm even after 35 scan cycles [8]. The cyclic voltammograms corresponding to the thiourea–molybdate-based film are presented in Figure 1-b. The first of the three CV deposition cycles exhibited two redox peaks (at –0.45 V and –0.5 V), which were very likely related to the formation of a molybdenum oxide layer on the bare electrode surface [5]. This behaviour was not observed during the later scans. Starting from the second sweep, the CVs do not exhibit the redox peaks that are typically observed during Mo–O–S film formation from an aqueous MoS_4^{2-} solution (Fig. 1-a). This can be considered the first indicator that this precursor mix $(NH_4)_6Mo_7O_{24}$ + $SC(NH_2)_2$ does not complex to form aqueous MoS_4^{2-} prior to electrodeposition and film formation, and probably proceeds via different a mechanism than that described in equations (1)–(3). This result may also be consistent with studies [20, 21] reporting the possibility of forming flower-like molybdenum sulfide nanostructures from thiourea and ammonium molybdate via a hydrothermal synthesis procedure without thiomolybdate ion intermediates. In particular, the group of Geng showed [20] that thiourea successfully supplied S to MoO_3 formed beforehand from $(NH_4)_6Mo_7O_{24}$.

An alternative film formation mechanism can be suggested based on the obtained results. The film formation likely occurs via the deposition of Mo–O species followed by electro-adsorption of the S ligand on the Mo–O covered FTO surface. This mechanism can be justified by the following arguments. Firstly, the possibility of the precursors chemically complexing to form aqueous MoS_4^{2-} can be preliminary rejected, as none of the characteristic visible solution features of MoS_4^{2-} were observed after mixing the thiourea and molybdate solutions. Secondly, we assume that the increase in the cathodic current at potentials more negative than –0.6 V can be attributed to the deposition of molybdenum oxide compounds. This step is predominantly associated with the electrodeposition of metals from aqueous solution at negative potentials accompanied by the parallel electrolysis of water rather than the reduction and deposition of aqueous S species (which were detected in this potential region when ATTM was used). Taking into account the complex solution chemistry of Mo(VI), cathodic electrodeposition is known to lead to nonstoichiometric and mixed valence molybdenum oxides, making the formulation of precise deposition mechanism impossible [5]. However, the electroreduction of molybdates can be expressed in a general way as follows [22]:

$$MoO_4^{-2} + 2H_2O + 2e^- \rightarrow MoO_2 + 4OH^- \quad (4)$$

We presume that this behaviour results in the FTO electrode being predominantly covered with Mo-O species. This type of surface should be negatively charged, according to the zeta potential data for Mo-oxo compounds [23]. It is well-established that thiourea can be electro-adsorbed on metals by S-head [19, 24, 25]. This process is electrochemically driven by the electrostatic forces between the electrolyte ions and the charged interfaces. Thus, the anodic peak at –0.7 V can be attributed to the electro-adsorption of TU on the negatively charged Mo–O surface. As aqueous thiourea is known to be positively charged (i.e. protonated) at the S atom (eq. (5)) [26], its electro-adsorption could be the dominant process occurring on the negatively charged Mo-O surface, producing a final layer of Mo–O–S structures on the FTO substrate.

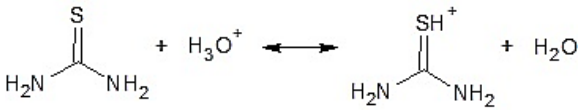

(5)

This thiourea behaviour slightly deviates from mechanism that would be expected based on the electrodeposition of an amorphous cobalt sulfide film using thiourea and cobalt salt as the S and Co precursors, respectively [27-30]; on the other hand, it corresponds well with the fundamentals of the formation of self-assembled (SA) monolayers of alkanethiols and S-donation through the electro-adsorption of the cleaved S-H thiol bond [19, 24, 31].

Finally, a homogeneous, brownish film that was visually identical to that produced from ATTM was formed on the FTO substrate as a result of the three continuous sweep cycles. The presence of Mo, O, and S was later confirmed by structural analysis, while the electrocatalytic properties of the film in the HER were compared with two benchmarks: the ATTM-based film and a Pt electrode.

3.2. Structural analysis

While ATTM-derived films have already been reliably characterized as amorphous structures containing the catalytically active species of MoS_{2+x} [6], the novel Mo–O–S films deposited from thiourea and molybdate bath were thoroughly characterized in this work. Moreover, the films were

annealed, and subsequently evaluated by structural analysis techniques. Thermal treatment can reduce "defects" in film composition, and may affect their overall catalytic activity.

Fig. 2 illustrates X-ray diffraction patterns recorded for the as-prepared and annealed Mo–O–S films that were electrodeposited on an FTO substrate from a thiourea and molybdate electrolyte using three sweep cycles. The absence of characteristic diffraction peaks for crystalline molybdenum oxide or sulfide suggested the existence of the amorphous phase or the lack of long-range crystalline order in the as-deposited films. Due to the poor crystallinity, only clearly defined SnO_2 (PDF 46–1088) peaks originating from the FTO substrate were detected. In contrast, additional peaks were observed in the XRD pattern of the annealed films, indicating a higher crystallinity than the as-deposited Mo–O–S samples. Analysis of the diffraction pattern led to the conclusion that the annealed film was composed predominantly of the α-MoO_3 phase (PDF 47-1320). In this regard, a variety of Mo oxide species are known to be present in the molybdenum oxides films, exhibiting diverse molecular structures such as Mo_8O_{26}, Mo_7O_{24}, or MoO_4 [32]. In addition to the peaks attributed to the Mo oxide species, diffraction signals characteristic of the small amount of the molybdenum sulfide phase were also present in the XRD pattern [20, 21].

The FT–IR spectra of the Mo–O–S samples are shown in Fig. 3. The absorption peaks at wavenumbers ca. 3400 cm^{-1} and 1630 cm^{-1} correspond to O–H stretching and bending vibrations, respectively. Electrodeposition using aqueous electrolytes usually leads to the formation of various oxo-intermediates. In this case, a series of absorption peaks at 1400, 880, and 740 cm^{-1} in the as-deposited films were assigned to various Mo–O bond vibrations [33]. The intensity of the latter peaks was greatly increased in the annealed sample. Although sulfur was barely observed in the crystallographic analysis, the IR spectra confirmed the presence of S bonds in the samples. The vibrations of the S–O bond can be seen at ca. 1000 cm^{-1}. Moreover, an absorption peak shoulder at around 480 cm^{-1} could be related to Mo–S stretching vibrations. The IR data suggested that the formation of the inorganic films was successful, as the characteristic peaks of thiourea functional groups [34] were absent in all the prepared samples.

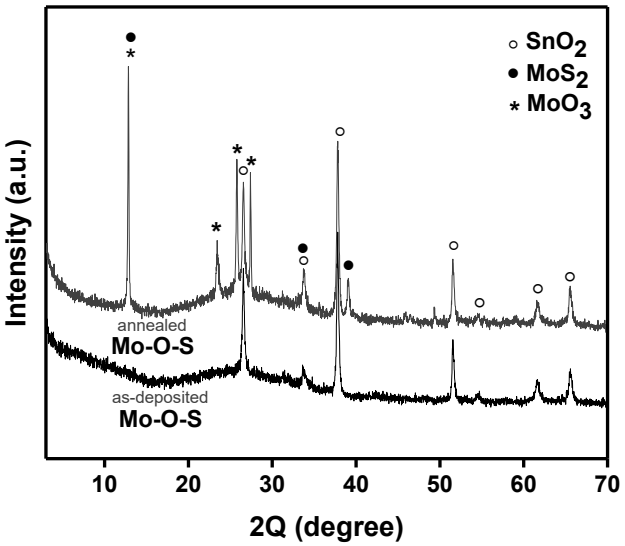

Figure 2. X-ray diffraction patterns of the as-deposited and annealed Mo–O–S films on FTO substrates

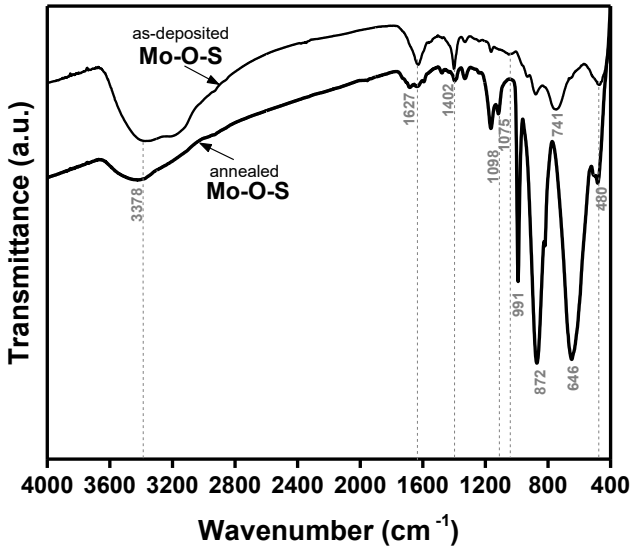

Figure 3. Characteristic FT-IR spectra of the as-deposited and annealed samples

SEM micrographs revealed the surface morphology of the prepared Mo–O–S films (Fig. 4). The as-deposited surface (Fig. 4 a, b) was relatively smooth, with small nodules and cracks. The presence of the cracks can be attributed to the generation of high internal stress during the drying-induced shrinkage [35]. Annealing at 623 K led to changes in film morphology and the formation of randomly oriented blocks (Fig. 4-c). Energy dispersive X-ray spectroscopy (EDX) was further employed to confirm the presence of Mo and S in the prepared films. The atomic ratio of Mo:S was determined to be approximately 1 by averaging the results of multiple measurements at different points on the film surface. However, it should be emphasized that the analysis also revealed variations in the Mo:S from 0.35–2 depending on the point under investigation. These results confirmed the high surface heterogeneity of the obtained films. In addition, a high oxygen content was detected in all the prepared samples. The oxygen was associated with the following sources: the presence of silica and tin oxides in the FTO substrate; the electrodeposition of molybdenum oxide/hydroxide films according to the electrochemical deposition mechanism described above; and the inevitable surface oxidation of Mo–O–S films by oxygen from the air.

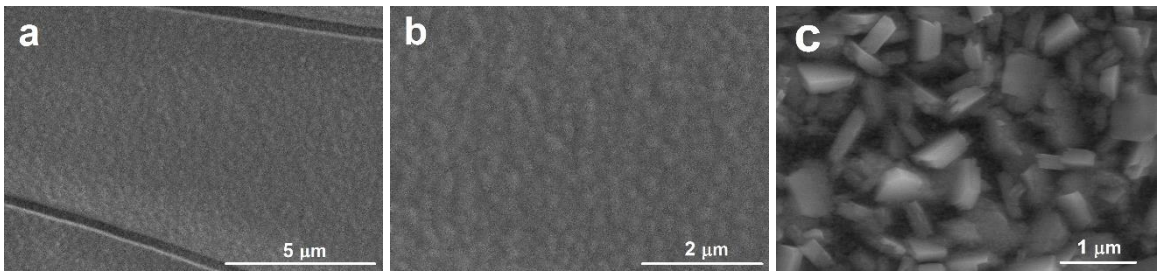

Figure 4. SEM images of the as-deposited (a, b) and annealed (c) Mo–O–S films

The Raman spectra presented additional information concerning the structure of the annealed Mo–O–S films (Fig. 5). The appearance of strong bands in the 800–1000 cm^{-1} region reflected the presence of the MoO_3 phase [36]. The Raman band at 994 cm^{-1} was associated with the symmetric stretching of the Mo=O bond. The band at 820 cm^{-1} was attributed to the asymmetric vibrations of the bridging Mo–O–Mo bonds, and the associated Mo–O–Mo bending mode was observed at ca. 150 cm^{-1} [36]. In most Raman spectroscopic studies of bulk MoS_2 samples, the active S–Mo–S modes are usually observed at 286, 383, and 408 cm^{-1} [37]. In our case, the observed Raman bands in the 250–400 cm^{-1} region could be partially related to the presence of Mo–S bonds. However, the applied analytical techniques did not unambiguously permit the identification of the exact structure and composition of the prepared films, as the signals associated with the Mo–O and Mo–S bonds can overlap.

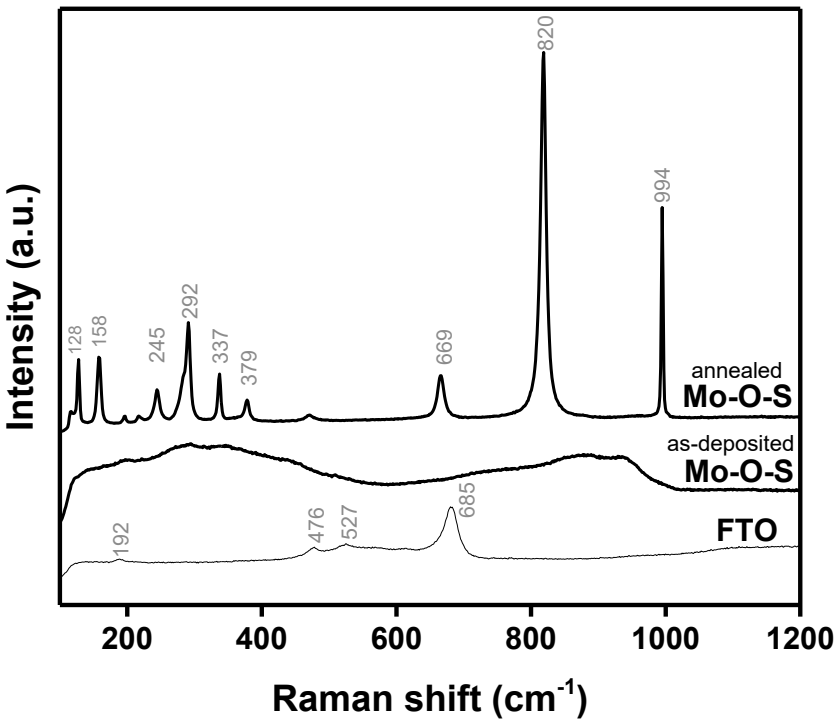

Figure 5. Raman spectra of the Mo–O–S films on FTO substrates

The UV-Vis diffuse reflectance spectra confirmed that the optical behaviour of the Mo–O–S films depended on the preparation conditions (Fig. 6). The as-deposited films exhibited a complex spectral response as well as strong absorption over the entire UV-Vis region. After annealing, the film became white in colour and exhibited increased light reflectance. A UV-Vis absorption edge energy of 3.88 eV was calculated from the rising part of spectrum.

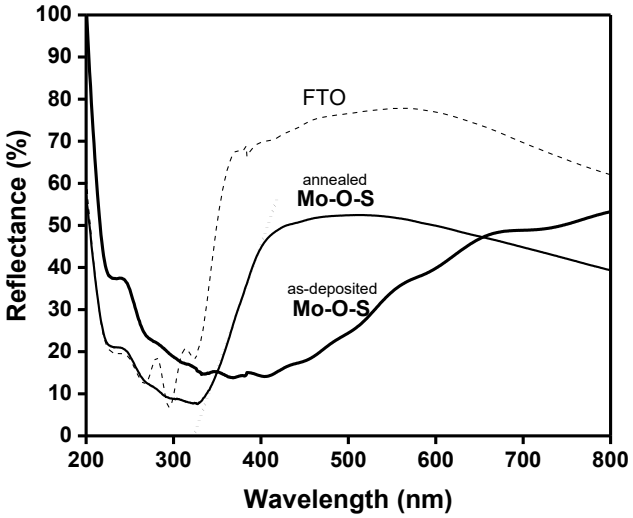

Figure 6. UV-Vis diffuse reflectance spectra of the Mo–O–S films on FTO substrates

3.3. Electrocatalytic activity in the HER

The catalytic performance of the Mo–O–S films in the HER reaction at pH 7 in a phosphate buffer solution was studied using a combination of chronopotentiometry and linear sweep voltammetry techniques. The galvanostatic method is known to be attractive for short-term electrochemical stability measurements when electrodes are tested under harsh current conditions [38], and 10 mA/cm^2 is known to be the current density required to produce industrial amounts of H_2 at low overpotentials. We tested our catalysts at half of the industrial value of 10 mA/cm^2 in order to simulate constant and intense H_2 evolution conditions, which are difficult to achieve in pH neutral solutions in typical *E-j* or *time-j* measurements. A current density of 5 mA/cm^2 has also been reported to be convenient to establish activity in the form of the reaction overpotential at a constant current density [39].

As reported above, annealing improved the crystallinity of the as-deposited films. However, it had a detrimental effect on their electrocatalytic activity in the HER. For this reason, only the experimental data for the as-deposited Mo–O–S films is included in the following discussion.

Figure 7 shows characteristic chronopotentiograms of the as-deposited Mo–O–S films at a constant applied cathodic current density of 5 mA/cm^2. As expected, the Mo–O–S film prepared from ATTM precursor was not immediately destabilized by the harsh electrolysis conditions with intense H_2 bubbling (Fig. 7-a). However, the overpotential required to produce a cathodic current density of 5 mA/cm^2 using this film was relatively high, and the reaction potential showed a tendency to increase due to the gradual dissolution of the ATTM-derived Mo–O–S film. The film sourced from molybdate and thiourea was also tested under the same HER conditions of 5 mA/cm^2 (Fig. 7-b). In contrast to the ATTM-derived film, our ATTM-free catalyst reached similar catalytic activity without noticeable film degradation. The potential did not change more than 20 mV during the whole electrolysis. These results showed the possibility for the catalyst prepared using thiourea and molybdate as Mo and S precursors to operate at the same rate as the reference ATTM-derived Mo–O–S film [8].

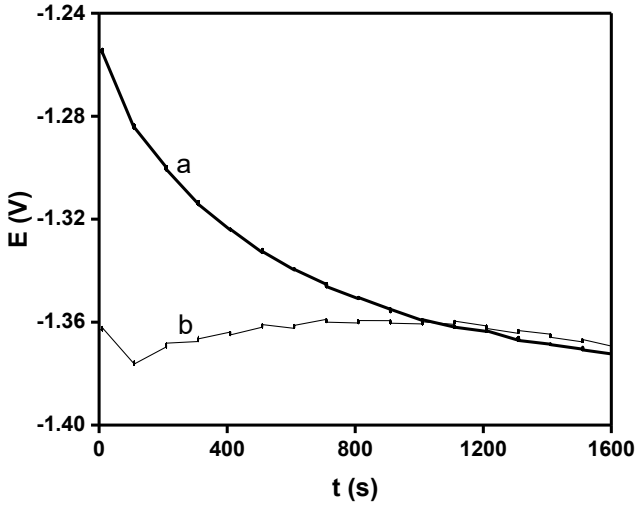

Figure 7. Characteristic chronopotentiograms recorded in a pH 7 phosphate buffer solution at a constant applied current density of 5 mA/cm^2 for the as-deposited Mo–O–S films prepared from (a) ATTM in $NaClO_4$ and (b) thiourea and ammonium molybdate solutions

Figure 8 represents the polarization curves of the ATTM-derived (Fig. 8-a) and thiourea-molybdate-based (Fig. 8-b) catalysts in pH 7 phosphate buffer solution. These catalysts were polarized from 0 V to –1 V before and after being used for electrolysis at 5 mA/cm^2 for 1600 s. This methodology allowed the changes to the films caused by the HER to be detected and compared, and therefore, for their stability in long-term operation under harsh HER conditions to be predicted. As can be seen, the HER started to occur at –0.8 V on the ATTM-derived Mo–O–S film (Fig. 8-a), while our thiourea-molybdate-based film demonstrated slow but constant current growth starting from less negative potentials (Fig. 8-b).

A Tafel analysis of the polarization curves of the Mo–O–S films prepared from the thiourea-molybdate precursors was carried out. The Tafel slopes in the range of $\eta \leq 100$ mV were found to be 91 mV·dec^{-1} and 85 mV·dec^{-1} for the films polarized before and after electrolysis at 5 mA/cm^2, respectively. These values corresponded well to those obtained for ATTM-based MoS_3 samples, which exhibited a Tafel slope of 86 mV·dec^{-1} at pH 7 polarization conditions [40]. Moreover, we noticed that the Tafel slope of the film was lower after intense HER operation. This result might not be a coincidence. Hu's group concluded that ATTM-based films undergo reductive activation during the HER, and all the different amorphous phases of the prepared films are transformed to the active catalytic species, MoS_{2+x} [9].

Both catalysts showed relatively low HER catalytic activity in pH 7 solution, as a current density of 1 mA/cm^2 was reached at overpotentials ≥ 300 mV. However, the results can be well compared for the current densities obtained at η=200 mV. In this case, ATTM-derived Mo–O–S film has a current density of 0.20 mA/cm^2 after being used for 5 mA/cm^2 electrolysis (Fig. 8-a). These results correlates well with the data reported for MoS_3 catalyst [40] with a current density of 0.19 mA/cm^2 at pH 7. An enhanced electrocatalytic behaviour can be seen for the Mo–O–S sample prepared from thiourea-molybdate bath in this work as the current density (0.42 mA/cm^2) (Fig. 8-b) is two times of that of ATTM

derived films. However, both the Mo–O–S films prepared in this work had a tendency to lose activity after electrolysis at 5 mA/cm^2, indicating the need for further modification of the films.

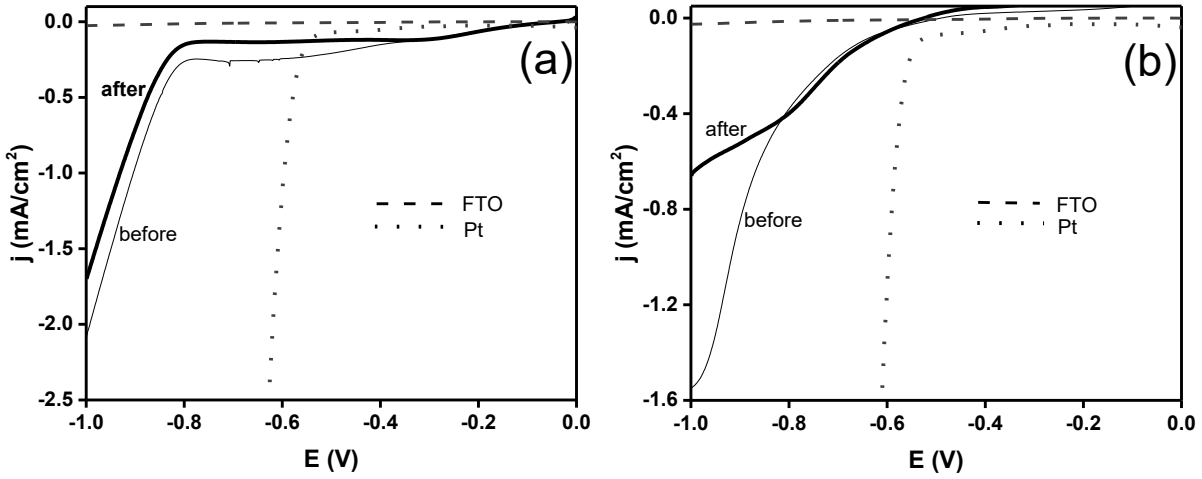

Figure 8. Polarization curves of the FTO/Mo–O–S electrodes in a 1.0 M phosphate buffer solution (pH 7) at a scan rate of 5 mV s^{-1} before and after 5 mA/cm^2 cathodic electrolysis. The Mo–O–S films were prepared from (a) ATTM in $NaClO_4$ and (b) thiourea and ammonium molybdate solutions

4. CONCLUSIONS

In summary, amorphous S-containing molybdenum oxide films have been successfully electrodeposited on an FTO substrate via cyclic voltammetry using thiourea and ammonium molybdate as the S and Mo precursors for the first time. The FTO electrode was cycled continuously from 0.2 V to –1.2 V until a thin layer of brownish film was deposited on the working electrode after three sweep cycles.

After extensive discussions, an alternative film formation mechanism was proposed, related to the Mo-O species deposition and subsequent electro-adsorption of the S ligand on the Mo-O covered FTO surface. The as-deposited amorphous films contained an extensive amount of oxygen, a relatively small amount of sulfur, had a thickness of 245 nm and a smooth and nodule-based surface. These samples were annealed, and improved crystallinity was observed via structural analysis techniques. However, thermal treatment had a detrimental effect on their electrocatalytic activity in the HER.

In contrast, the as-deposited amorphous Mo–O–S films showed enhanced electrocatalytic behaviour for hydrogen evolution at pH 7. In this case, a constant applied cathodic current density of 5 mA/cm^2 was employed to simulate prolonged and intense H_2 bubbling conditions. The results demonstrated that the thiourea-molybdate-based films operated at the same rate as the reference and the well-defined ATTM-derived Mo–O–S films in a pH 7 phosphate buffer solution. We introduce our catalyst as attractive material based on cheap and abundant alternative precursors for cost-effective pH neutral HER systems.

References

1. A. Züttel, A. Borgschulte, L. Schlapbach, Hydrogen as a Future Energy Carrier, Wiley-VCH, 2008.
2. A. Godula-Jopek, Hydrogen Production: by Electrolysis, Wiley-VCH, 2015.
3. I. Dincer, C. Acar, *Int. J. Hydrogen Energy*, 40 (2015) 11094.
4. P.D. Tran, T.V. Tran, M. Orio, S. Torelli, Q.D. Truong, K. Nayuki, Y. Sasaki, S.Y. Chiam, R. Yi, I. Honma, J. Barber, V. Artero, *Nat. Mater.*, 15 (2016) 640.
5. V.S. Saji, C.W. Lee, *ChemSusChem*, 5 (2012) 1146.
6. C.G. Morales-Guio, X. Hu, *Acc. Chem. Res.*, 47 (2014) 2671.
7. M. Bouroushian, Electrochemistry of Metal Chalcogenides, Springer, 2010.
8. D. Merki, S. Fierro, H. Vrubel, X. Hu, *Chem. Sci.*, 2 (2011) 1262.
9. H. Vrubel, X. Hu, *ACS Catal.*, 3 (2013) 2002.
10. C.G. Morales-Guio, L. Liardet, T.M. Mayer, S.D. Tilley, M. Grätzel, X. Hu, *Angew. Chem. Int. Ed.*, 54 (2014) 664.
11. S. Murugesan, A. Akkineni, B.P. Chou, M.S. Glaz, D.A. Vanden Bout, K.J. Stevenson, *ACS Nano*, 7 (2013) 8199.
12. A.S. Aliyev, M. Elrouby, S.F. Cafarova, *Mater. Sci. Semicond. Process.*, 32 (2015) 31.
13. B. Kendall, T.W. Dahl, A.D. Anbar, *Reviews in Mineralogy and Geochemistry*, 82 (2017) 683.
14. S. Chandra, S.N. Sahu, *J. Phys. D: Appl. Phys.*, 17 (1984) 2115.
15. N. Dukstiene, K. Kazancev, I. Prosicevas, A. Guobiene, *J. Solid State Electrochem.*, 8 (2004) 330.
16. E.A. Ponomarev, M. Neumann-Spallart, G. Hodes, C. Lévy-Clément, *Thin Solid Films*, 280 (1996) 86.
17. S.K. Ghosh, T. Bera, O. Karacasu, A. Swarnakar, J.G. Buijnsters, J.P. Celis, *Electrochim. Acta*, 56 (2011) 2433.
18. Q. Li, E.C. Walter, W.E. van der Veer, B.J. Murray, J.T. Newberg, E.W. Bohannan, J.A. Switzer, J.C. Hemminger, R.M. Penner, *J. Phys. Chem. B*, 109 (2005) 3169.
19. O. Azzaroni, G. Andreasen, B. Blum, R.C. Salvarezza, A.J. Arvia, *J. Phys. Chem. B*, 104 (2000) 1395.
20. X. Wang, J. Ding, S. Yao, X. Wu, Q. Feng, Z. Wang, B. Geng, *J. Mater. Chem. A*, 2 (2014) 15958.
21. K. Pandey, P. Yadav, D. Singh, S.K. Gupta, Y. Sonvane, I. Lukačević, J. Kim, M. Kumar, *Sci. Rep.*, 6 (2016) 32690.
22. S.F. Cafarova, A.S. Aliyev, M. Elrouby, N. Soltanova, D.B. Tagiyev, *J. Electrochem. Sci. Eng.*, 5 (2015) 231.
23. E. Skwarek, S. Khalameida, W. Janusz, V. Sydorchuk, N. Konovalova, V. Zazhigalov, J. Skubiszewska-Zięba, R. Leboda, *J. Therm. Anal. Calorim.*, 106 (2011) 881.
24. V. Brunetti, B. Blum, R.C. Salvarezza, A.J. Arvia, P.L. Schilardi, A. Cuesta, J.E. Gayone, G. Zampieri, The *J. Phys. Chem. B*, 106 (2002) 9831.
25. G. García, J.L. Rodríguez, G.I. Lacconi, E. Pastor, *Langmuir*, 20 (2004) 8773.
26. M. Özcan, İ. Dehri, M. Erbil, *Appl. Surf. Sci.*, 236 (2004) 155.
27. R. Mardosaite, E. Valatka, *Chalcogenide Lett.*, 14 (2017) 171.
28. U.K. Sultana, T. He, A. Du, A.P. O'Mullane, *RSC Adv.*, 7 (2017) 54995.
29. N. Kornienko, J. Resasco, N. Becknell, C.M. Jiang, Y.S. Liu, K. Nie, X. Sun, J. Guo, S.R. Leone, P. Yang, *J. Am. Chem. Soc.*, 137 (2015) 7448.
30. Y. Sun, C. Liu, D.C. Grauer, J. Yano, J.R. Long, P. Yang, C.J. Chang, *J. Am. Chem. Soc.*, 135 (2013) 17699.
31. C. Nicosia, J. Huskens, *Mater. Horiz.*, 1 (2014) 32.
32. I. A. de Castro, R. S. Datta, J. Z. Ou, A. Castellanos-Gomez, S. Sriram, T. Daeneke, K. Kalantar-zadeh, *Adv. Mater.*, 29 (2017) 1701619.
33. N. Maheshwari, G. Muralidharan, *Appl. Surf. Sci.*, 416 (2017) 461.
34. V. Kumar, R. Sundararajan, *J. Miner. Mater. Char. Eng.*, 3 (2015) 118.

35. R.S. Patil, M.D. Uplane, P.S. Patil, *Appl. Surf. Sci.*, 252 (2006) 8050.
36. H. Tian, C.A. Roberts, I.E. Wachs, *J. Phys. Chem. C*, 114 (2010) 14110.
37. B.C. Windom, W.G. Sawyer, D.W. Hahn, *Tribol. Lett.*, 42 (2011) 301.
38. E.J. Popczun, J.R. McKone, C.G. Read, A.J. Biacchi, A.M. Wiltrout, N.S. Lewis, R.E. Schaak, *J. Am. Chem. Soc.*, 135 (2013) 9267.
39. J. Staszak-Jirkovský, C.D. Malliakas, P.P. Lopes, N. Danilovic, S.S. Kota, K.C. Chang, B. Genorio, D. Strmcnik, V.R. Stamenkovic, M.G. Kanatzidis, N.M. Markovic, *Nat. Mater.*, 15 (2015) 197.
40. D. Merki, H. Vrubel, L. Rovelli, S. Fierro, X. Hu, *Chem. Sci.*, 3 (2012) 2515.